Gu *et al. Chem Synth* 2023;3:21
DOI: 10.20517/cs.2023.08

Chemical Synthesis

Research Article

Open Access

Nanodiamond derived N-doped sp^3@sp^2 hybrid carbocatalysts for the aerobic oxidative synthesis of 2-substituted benzoxazoles

Qingqing Gu[1], Rui Huang[2], Chi Xu[1], Shiyan Li[1,3], Siglinda Perathoner[4], Gabriele Centi[4], Yuefeng Liu[1,*]

[1]Dalian National Laboratory for Clean Energy (DNL), Dalian Institute of Chemical Physics, Chinese Academy of Sciences, Dalian 116023, Liaoning, China.
[2]Zhang Dayu School of Chemistry, Dalian University of Technology, Dalian 116024, Liaoning, China.
[3]University of Chinese Academy of Sciences, Beijing 100049, China.
[4]Dept.s ChiBioFarAm and MIFT, University of Messina, V. le F. Stagno D'Alcontres 31, Messina 98166, Italy.

***Correspondence to:** Dr. Yuefeng Liu, Dalian National Laboratory for Clean Energy (DNL), Dalian Institute of Chemical Physics, Chinese Academy of Sciences, 457 Zhongshan Road, Dalian 116023, Liaoning, China. E-mail: yuefeng.liu@dicp.ac.cn

How to cite this article: Gu Q, Huang R, Xu C, Li S, Perathoner S, Centi G, Liu Y. Nanodiamond derived N-doped sp^3@sp^2 hybrid carbocatalysts for the aerobic oxidative synthesis of 2-substituted benzoxazoles. *Chem Synth* 2023;3:21. https://dx.doi.org/10.20517/cs.2023.08

Received: 15 Feb 2023 **First Decision:** 15 Mar 2023 **Revised:** 25 Mar 2023 **Accepted:** 7 Apr 2023 **Published:** 28 Apr 2023

Academic Editor: Bao-Lian Su **Copy Editor:** Yanbing Bai **Production Editor:** Yanbing Bai

Abstract

Carbocatalysts, as a member of metal-free catalysts, have shown promising potentials in many catalytic transformations in the past few decades. Nitrogen doping has been identified as an effective way to tailor the properties of carbocatalysts and render their potential use for various applications. It is also important to fabricate unique surface compositions or properties for the N species to enhance their intrinsic catalytic activities. Hybrid sp^3@sp^2 nanocarbons, from this perspective, could enhance catalytic activity by tuning the electronic structure of the active sites. Herein, N-doped sp^3@sp^2 hybrids were prepared from nanodiamonds (NDs) and $(NH_4)_2CO_3$ as starting N precursor to dope the NDs and tune their sp^3/sp^2. The N-doped sp^3@sp^2 hybrid nanocarbons were studied in the oxidative catalytic synthesis of a broad series of drug-related compounds (23 examples of 2-substituted benzoxazoles, benzothiazoles and benzimidazoles). These catalysts show high catalytic activity and reusability in mild conditions. Their performances are comparable to homogeneous/heterogeneous metal-based catalysts. The pyridinic N species determine the enhancement in the catalytic performance. The mechanistic results indicate that the N-doped sp^3@sp^2 hybrid activates oxygen molecules to form $O_2^{\bullet-}$ as reactive oxygen species, which abstracts the proton attached on the catalyst's surface. This study provides an attractive and useful methodology for applying ND-derived carbocatalysts to synthesise 2-substituted benzoxazoles and more complex drug targets.

Keywords: Carbocatalysis, N-doped sp^3@sp^2 hybrids nanocarbon, metal-free catalyst, aerobic liquid-phase reaction, drugs intermediate synthesis

INTRODUCTION

Nanocarbons are emerging as competitive candidates for conventional metal-based catalysts over the past few decades owing to their fascinating physicochemical properties and metal-free nature[1-3]. Chemical doping (e.g., N or B) is an efficient strategy to regulate the catalytic activity of nanocarbon since it could induce charge transfer and redistribution between doping sites and neighbouring carbon and thus enhance the catalytic performance of nanocarbon[4-6]. For N-doped carbon-based metal-free catalysts, the different N-bonding environment renders various nitrogen species (i.e., pyridinic nitrogen, pyrrolic nitrogen, and graphitic nitrogen) with different intrinsic catalytic performance[7,8]. Furthermore, it was also identified that the topological vacancy defects in the adjacent positions of N species or unique surface compositions (e.g., sp^3@sp^2 hybrid carbon surface) could boost the nitrogen species with enhanced catalytic activities[9].

Among the most developed nanocarbon materials, sp^3-hybridized nanodiamonds (NDs) and their derivatives with unique surface energy, electronic structure, high curvature and tunable sp^3/sp^2 carbon ratios can offer a wide range of possibilities for an advanced design of catalytic sites[10-15]. In particular, the outer sphere of the NDs could gradually transform into curved graphitic-like shells, forming sp^3@sp^2 hybrid nanocarbon with a sp^3 carbon core covered with a few graphitic-like shells by high-temperature annealing under vacuum or inert atmosphere[16]. The functionalization and heteroatom doping could further enrich the catalytic chemistry by introducing acid/base or redox catalytic sites[17]. sp^3@sp^2 hybrid nanocarbons have been proven to be efficient catalysts for various liquid-phase reactions[18-22], but their applications in pharmaceutical synthesis have rarely been reported.

Five-membered heterocyclic rings, such as benzoxazoles, benzothiazoles and benzimidazoles, are important building blocks for natural products, bioactive molecules, and pharmaceutical and agrochemical compounds[23,24]. Aminoxyl radicals (e.g., 4-methoxy-TEMPO[23]), metal complexes [Ru-xantphos[24], CuI/TEMPO/Bpy[25], $Zn(OAc)_2$[26], etc.] and metal nanoparticles (Au/TiO_2[27], Pt nanocluster[28], $AgPd/WO_{2.72}$[29], etc.) have been proved to be efficient catalysts for the aerobic catalytic synthesis of benzoxazole framework. Their catalytic activities originate from the agostic interaction endowed by their strong electron-acceptor/donor properties, which could efficiently facilitate the hydrogen abstraction process (a key reaction step for the synthesis of benzoxazoles). Regardless of the progress made in metal-based catalysts, many issues are still present in catalyst recovery, costs and stability, and especially metal leaching during the reaction. In addition, for the use of these products in many pharmaceutical applications, the presence of residual metals, even at ppb levels, must be avoided. Hence, it is desirable to develop efficient and metal-free synthetic strategies for heterogeneous aerobic catalytic synthesis of heterocycles. Nanocarbons offer from this perspective unique characteristics, and they have been demonstrated in various catalytic reactions[2,30-34]. Kawashita *et al.* found that activated carbon could catalyze the direct synthesis of 2-arylbenzoxazoles efficiently; however, the unclear role of activated carbon retards the deep understanding of the reaction mechanism and the rational design of more efficient carbocatalysts[35].

Therefore, the development of N-doped sp^3@sp^2 hybrid carbon catalysts for the synthesis of pharmaceuticals is much desired and promising because a) exploring the feasibility of carbocatalysts for the synthesis of benzoxazoles would expand their applications in the pharmaceutical industry; b) sp^3@sp^2 hybrid nanocarbons exhibit remarkable hydrogen-abstraction ability in the case of oxidative dehydrogenation reactions[34,36] and oxidation of benzyl alcohol[20], indicating they are operative in the synthesis of

benzoxazoles; c) the use of nonmetal catalysts can lower the cost and environmental footprint and avoid the metal leaching during the reaction, which is very important for the pharmaceutical industry; d) the catalysts can be readily separated and reused due to their heterogeneous nature.

We report herein the first general strategy for the aerobic synthesis of benzoxazoles with o-aminophenol and benzaldehyde catalyzed by N-doped sp^3@sp^2 hybrid nanocarbon [Scheme 1] NDs and $(NH_4)_2CO_3$ was chosen as starting material and N precursor and the surface properties of N-doped sp^3@sp^2 hybrid could be tuned during the synthesis process. These derived N-doped sp^3@sp^2 hybrid nanocarbon are characterized by N-doped sp^2 C layers (graphene-like) surrounding an sp^3 C-core[12,23], which is confirmed by high-resolution transmission electron microscopy (HR-TEM), Raman, X-ray photoelectron spectroscopy (XPS) and electron energy loss spectroscopy (EELS). These derived N-doped sp^3@sp^2 hybrid nanocarbon show high selectivity, yields and wide substrate scope under mild operation conditions. This study provides an attractive and useful methodology to apply carbocatalysts for the synthesis of 2-substituted benzoxazoles and more complex drug intermediates.

EXPERIMENTAL

Synthesis of N-doped sp^3@sp^2 hybrid nanocarbon

The NDs were purchased from the Beijing Grish Hitech Co. and purified by concentrated HCl (37%) solution under room temperature six times (12 h per time) to remove metal impurities from NDs. After being washed thoroughly with DI water until neutral pH, the samples were dried in a vacuum oven at 60 °C. In a typical preparation of N-doped sp^3@sp^2 hybrid nanocarbon, 1.5 g of citric acid (99.5%, Sinopharm) and 1.5 g $(NH_4)_2CO_3$ (Analytical Grade, Sinopharm) were dissolved in 5 mL distilled water, followed by an addition of 1.0 g of purified NDs and ultrasonication was applied for 30 min to achieve uniform dispersion. Then, the obtained mixture was cured in an oven at 130°C for five h, followed by thermal treatment at 900 °C under an Ar atmosphere for two h (3 °C /min). The obtained samples were named NND900. ND900 was obtained by annealing purified NDs at 900 °C under an Ar atmosphere for two h (3 °C /min). ND900 was oxidized by H_2SO_4 and HNO_3 (1:1) under 105 °C for four h to form oND900. NoND900 was obtained by annealing oND900 under 550 °C in pure NH_3 for 4h.

Typical procedure for the aerobic synthesis of 2-substituted benzoxazoles

The reactions were performed in pressure tubes. Aminophenol (2 mmol), benzaldehyde (2.2 mmol), 120 mg catalysts and 10 mL of xylene as solvent were added into the 75 mL glass pressure tube, followed by an exchange with O_2. Then the tube was sealed and maintained at 140 °C for a certain time. After completing the reaction, the tube was cooled to room temperature and 10 ml EtOH and 200 μL nitrobenzene were added for quantitative analysis with GC (Agilent 7,820 with HP-5 column). For the recycling test, the used catalysts were filtrated and then washed by EtOH. Then the new reactants and solvent were added for the next run. The catalysts were filtrated for the substrate scope experiment, and the reaction liquid was rotary evaporated to isolate the product.

Characterization

The XPS measurements were performed using a Thermo Scientific ESCALAB 250Xi instrument equipped with Al Kα excitation source; Metal content of the samples was determined by inductively coupled plasma optical emission spectrometer (ICP-OES, PerkinElmer 7300DV); HR-TEM analysis for ND-based catalysts was conducted on Titan Themis ETEM G3 microscope with image corrector at 300 kV and Hitachi HF5000 with aberration-corrector at 200 kV. The EELS analyses were performed on the STEM model on a Hitachi HF5000 microscope with a probe corrector at 200 kV cold-field emission gun. The energy resolution for the EELS system is better than 60 meV, which is determined from full-width at half-maximum (FWHM) of the zero-loss peak. Raman spectroscopy was conducted on Renishaw (NanoWizard) with 325 nm laser

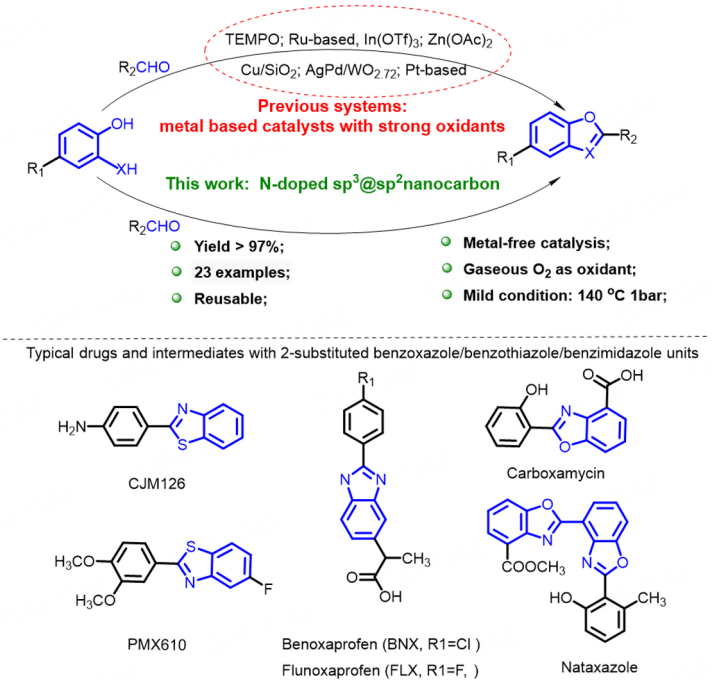

Scheme.1 (Top) A summary of the main routines for synthesising 2-substituted benzoxazoles, benzothiazoles and benzimidazoles. (Bottom) Examples of drugs containing 2-substituted benzoxazoles, benzothiazoles or benzimidazoles motif.

excitation and a power of 0.1 mW. Electron Paramagnetic Resonance (EPR) measurements were performed with an EPR X-band spectrometer (Bruker A200) at RT with samples sealed in a quartz sample tube. UV-vis absorption spectrum was obtained by UV-vis spectrometer (SHIMADZU UV2,600).

Detecting superoxide radical anion

Typical spectrometer parameters were: microwave power 20 mW, microwave frequency 9.4 GHz, scan time 60s, modulation amplitude 0.02 mT, modulation frequency 100 kHz. For the EPR test, 5, 5-dimethyl-1-pyrroline N-oxide (DMPO) was used as a radical trapper and dissolved in EtOH to prepare 20 mg/mL DMPO solution. The different reactions were performed as described above. After 2 h of reaction, the reaction solution was quickly taken out into a small tube and added DMPO solution. Then the mixture was measured by EPR.

Detecting H_2O_2

The evolved H_2O_2 in the catalytic process was measured using the colourimetric DPD method. The DPD method is based on the oxidation of N, N-diethyl-phenylenediamine (DPD) catalyzed with horseradish peroxides (POD) by H_2O_2. Briefly, 0.1 g of DPD was dissolved in 10 mL H_2O, denoted as solution A. 0.1 mg peroxidase (POD) was dissolved in 10 mL water, designated as solution B. After the reaction, 10 mL H_2O was added to the reaction solution and the mixture was further stirred thoroughly to extract the H_2O_2 from the organic phase to the water. After the stirring, the H_2O_2-containing water was separated from the organic solvent. Then 0.5 mL water was token and further diluted with 4 mL DI water, denoted as solution C. Finally, 4.5 mL solution C, 0.5 mL phosphorous buffer solution (pH 6.7), 10 μL solution A, and 10 μL solution B were mixed for the e ultraviolet-visible spectra test.

RESULTS AND DISCUSSION

Preparation and structural identification of N-doped sp^3@sp^2 nanocarbon

As illustrated in Figure 1A, the N-doped sp^3@sp^2 hybrid nanocarbon (NND900) was prepared by annealing ND at 900 °C under Ar with nitrogen precursor. A typical TEM image of the NDs particles in Supplementary Figure 1A reveals that the spacing of the lattice fringe is about 0.206 nm, which agrees well with (111) planes of diamond. After the nitrogen doping and the subsequent annealing, the diamond core was covered by 1-2 sp^2 C layers NND900, [Figure 1B and Supplementary Figure 1B]. The introduction of N species and homogeneity of the catalyst were confirmed by energy-dispersive X-ray spectroscopy (EDS) elemental mapping results [Figure 1C]. The XPS spectrum in the region of N1s reveals that the surface N content of NND900 increased to 3.7 at% [Figure 1D]with four configurations, including pyridinic N (N1, 398.5 eV), pyrrolic N (N2, 400.1 eV), graphitic N (N3, 401.1 eV) and N oxide (N4, 403.2 eV)[37]. XPS C1s spectra [Figure 1D and Supplementary Table 1] present that the sp^2/sp^3 value of NND900 increased to 0.5 from 0.2 of NDs, indicating the transformation of sp^3 C to sp^2 C during the synthesis process.

The Raman also studied the structure evolution of catalysts, as shown in Figure 1E and Supplementary Table 2, the spectrum of NDs exhibits a peak at 1,622 cm^{-1} (G band at 1,590 cm^{-1} and OH bending vibrations at 1,640 cm^{-1}) and diamond sp^3 mode at 1,324 cm^{-1}. After nitrogen doping and annealing, the decreased diamond peak and the forming of a broad D-mode (around 1,364 cm^{-1}) were observed, which originated from the breathing of hexagonal carbon rings with defects, were observed. Meanwhile, the G-mode peak is sharpened and shifted from 1,622 cm^{-1} to 1,587 cm^{-1}, which indicates the transformation of sp^3-hybridized C into sp^2-hybridized C and the graphitization of sp^2 C. The EELS results [Figure 1F] also confirm this transformation since the intensity of π^* peak (285 eV, for sp^2 C) increased after annealing and the addition of N precursor[13]. These results clarify the evolution process of sp^3 hybridization C transformed into sp^2 hybridization C and the successful introduction of N species into the sp^3@sp^2 nanocarbon surface.

Catalytic performance of N-doped sp^3@sp^2 hybrid nanocarbon

The aerobic synthesis of 2-phenyl benzoxazole (P, target product) by o-aminophenol A and benzaldehyde B was chosen as the model reaction [see the top of Figure 2] to explore the catalytic performance of ND-based nanocarbons catalysts. Without the catalyst [Figure 2A], 96.1% of A could be exclusively converted into I (2-benzylidene amino phenol, intermediate) with 99.8% selectivity, but the desired product P was undetected. The condensation reaction between the amino-group A and aldehyde-group B occurs easily without a catalyst, while the dehydrogenation and annulation steps between the -OH group and the imide C-H bond of I require a catalyst.

When used as a catalyst, the pristine NDs (i.e., before N introduction) give only traces of P [Figure 2A]. After the oxygen groups were introduced by HNO_3/H_2SO_4 treatment (oND900), the catalytic performance was not affected significantly. NND900 catalyst instead shows a remarkably enhanced formation of P 9.6%, structure confirmed by GC-MS, ^{1}H-NMR and ^{13}C-NMR in [Figure 2B and Supplementary Figure 2], indicating the important role of N doping. The low catalytic activity of NoND900 (selectivity 1.2% of P) implies the limited nitrogen introduction ability of NH_3 post-treatment. As shown in Supplementary Table 3, the surface area of NDs is 321 $m^2 \cdot g^{-1}$. After oxidation by HNO_3/H_2SO_4 (oND900) and subsequent NH_3 post-treatment (NoND900), the surface area increases to 360 $m^2 \cdot g^{-1}$. The surface area of NND900 is 366 $m^2 g^{-1}$, similar to that of oND900 and NoND900. Since the NND900 shows much better catalytic activity than NoND900 [Figure 2A], it may be excluded that the differences in the catalytic behaviour depend on the surface area.

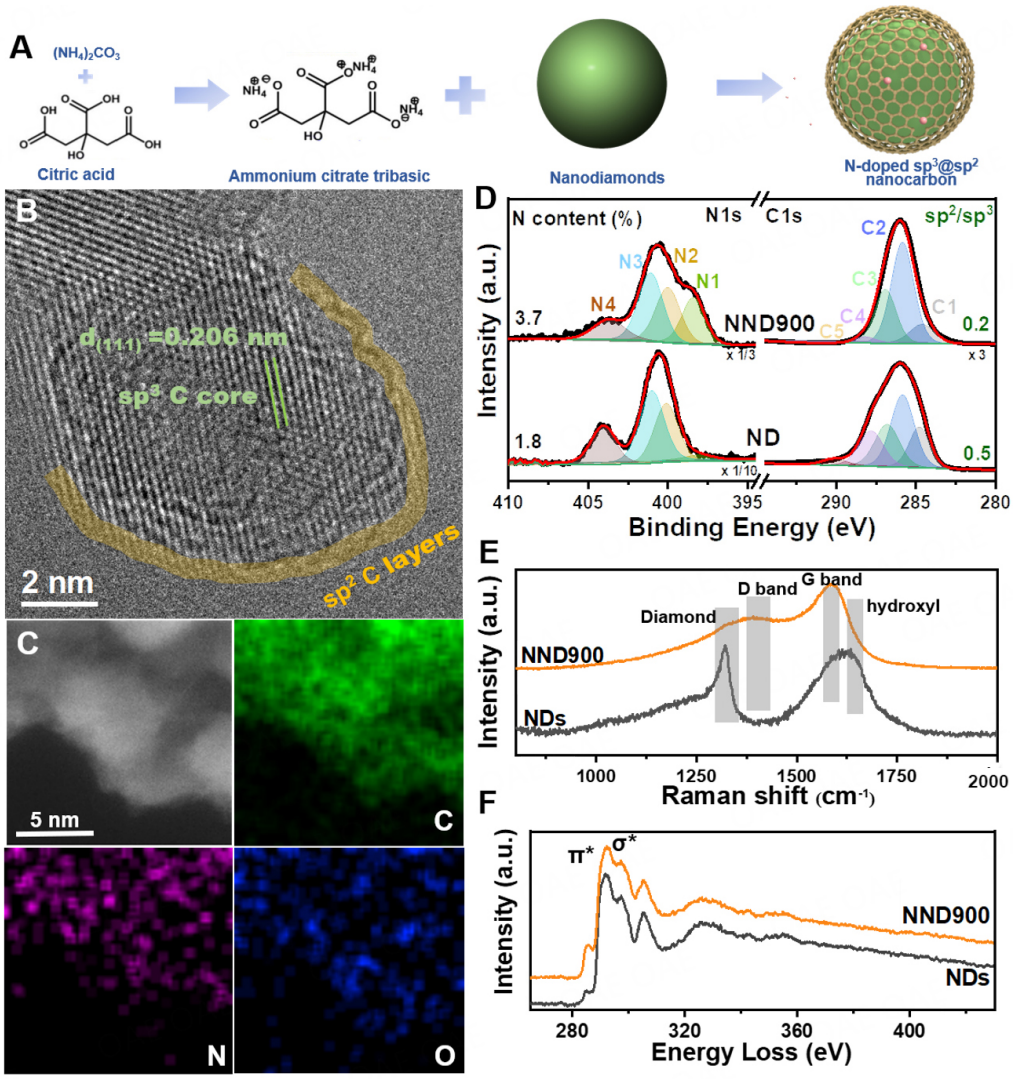

Figure 1. A:The strategy of fabricating N-doped sp^3@sp^2 nanocarbon; B: Representative HR-TEM image; C: EDS elemental mapping of NND900; D: XPS spectrum in N1s and C1s regions of NDs and NND900, C1: sp^2 C; C2: sp^3 C; C3: C-O, C-N; C4: C = O; C5: O-C = O; N1: pyridinic N; N2: pyrrolic N; N3: graphitic N; N4: N oxide; E: Raman spectra (λ = 325 nm) of NDs and N-doped sp^3@sp^2 nanocarbon; F: EELS profiles of NDs and N-doped sp^3@sp^2 nanocarbon.

Note that substituting O_2 in the reaction atmosphere with N_2, no product P was detected, indicating that O_2 is indispensable to the dehydrogenation step of I [Figure 2A]. To optimize the performances and understand better the catalytic behaviour, the role of reaction temperature and time were further investigated [Figure 2A and Supplementary Table 4]. The selectivity of P increases with reaction time and reaches the value of 97.4% at 28 h. The catalyst mass normalized formation rate of product P (r_P) could reach 2.3 mmol $h^{-1}g^{-1}$, comparable with the reported homogeneous or heterogeneous metal-based catalytic systems and the reported conventional active carbon [Supplementary Table 5]. Furthermore, the catalyst could be applied to five successive reaction cycles with negligible loss of the catalytic efficiency [1st yield P of 79.0% *vs.* 5th yield P of 77.1%, Figure 2C].

Given that similar catalytic performance of further purified NND900-HCl and extra Fe-loaded Fe/NND900 samples to NND900 [Supplementary Table 6], the possible contribution of residual metal impurities can be

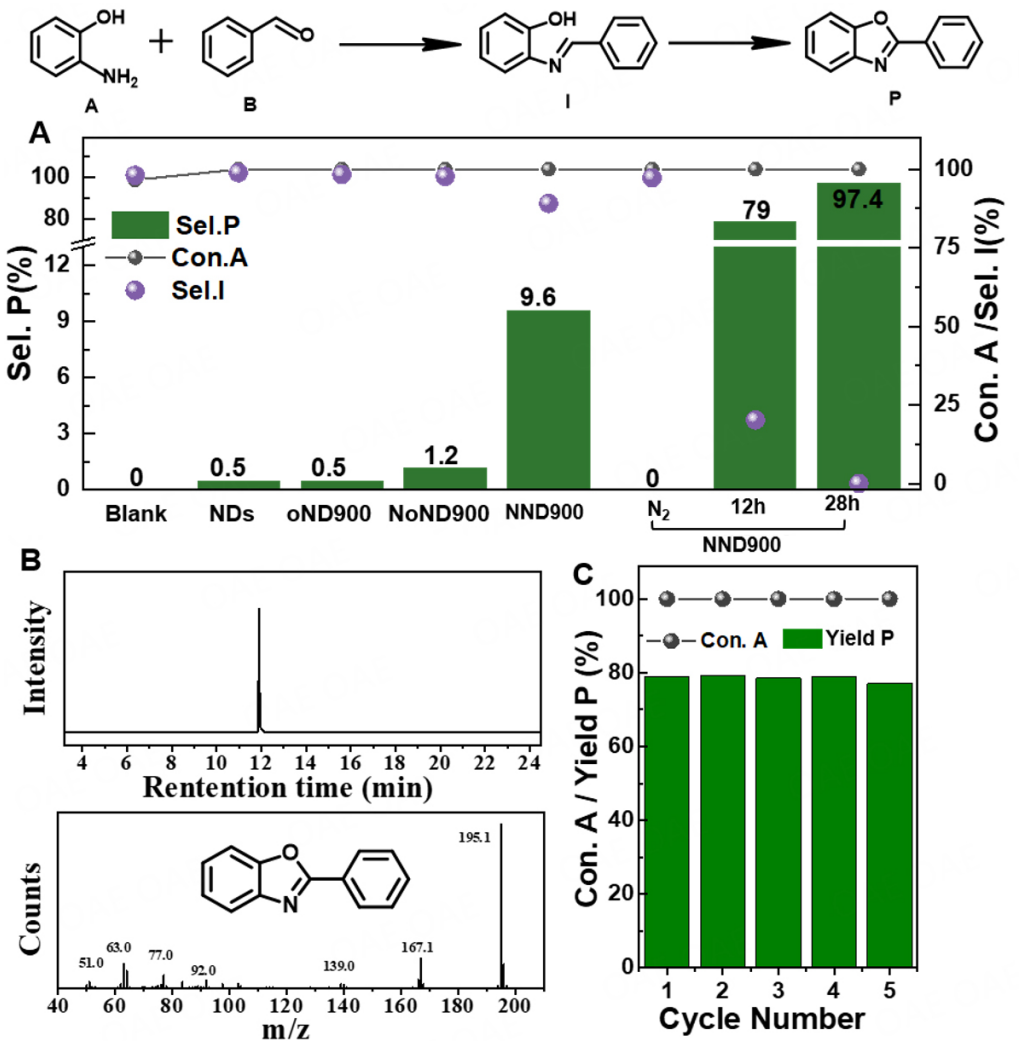

Figure 2. A: Catalytic performance of different NDs-based catalysts; 2 mmol aminophenol, 2.2 mmol benzaldehyde, 10 mL xylene, 40 mg catalyst, 140 °C, t = 2 h, 1 bar O_2; Quantitative analysis was carried out by GC using nitrobenzene as internal standard; B: Product structure identification by GC-MS; C: Plot of conversion of aminophenol and yield of 2-phenyl benzoxazole after five runs on NND900; 2 mmol 2-aminophenol; 2.2 mmol benzaldehyde; 10 mL xylene; 120 mg catalyst; T = 140 °C; Time = 12 h.

excluded [confirmed by ICP results in Supplementary Table 7].

The potential influence of carbon debris on the catalytic activity could also be excluded by comparing the catalytic performance of different temperature-annealed NDs. As shown in Supplementary Figure 3, the yield of P increases from 0.5 to c.a. 7 when annealing the NDs under 900 °C, 1,300 °C and 1,600 °C, implying the formed sp^2 layers may also be positive to the catalytic activity while the carbon debris does not contribute to the catalytic activity.

These results indicate that the intrinsic catalytic activity originates from the nanocarbon rather than the residual metal species or the carbon debris. According to the XPS N1s analysis results in Supplementary Table 8, the pyridinic N percentage (N1/N) of NND900 increases to 22.5% compared to 2.7% of NDs and 3.9% of ND900. In contrast, other N species' percentages in NND900 remain similar or decrease compared to the NDs and ND900.

The 1,10-phenanthroline and carbazole, as pyridinic-bearing and pyrrole-bearing aromatic compounds, respectively, were further chosen to study their catalytic performance. As shown in Supplementary Table 9, 1,10-phenanthroline shows a 13.7% yield of P. In comparison, carbazole shows a 7.0 % yield of P, indicating that aromatic compounds with pyridine structure are more active for the aerobic oxidative synthesis of 2-phenyl benzoxazole. This indicates a critical role of pyridinic N in the catalytic activity for the aerobic synthesis of 2-phenyl benzoxazole.

Mechanism study

The spin-trapping electron paramagnetic resonance (EPR) technique using 5,5-dimethyl-1-pyrroline N-oxide (DMPO) as the spin trap was performed to obtain information on the activation process of O_2[38]. As shown in Figure 3A, the catalytic systems with a substrate and catalyst or a mixture of substrate and O_2 remain EPR silent after adding DMPO. When substrate, catalyst and O_2 were all presented, the EPR signal of the catalytic system shows the characteristic fingerprint of spin adducts DMPO-•OOH compared with the simulated DMPO-•OOH EPR signal, which resulted from trapping superoxide (O_2•$^-$) with DMPO[39]. The results indicate the O_2 activation by N-doped sp^3@sp^2 nanocarbon and the generation of reactive $O_2^{\bullet-}$ species, which could be responsible for the oxidative dehydrogenation steps during P synthesis. It is reasonable to speculate that the H_2O_2 would be formed as an intermediate in the $O_2^{\bullet-}$ involved aerobic oxidation reactions. To proven this hypothesis, the detection of H_2O_2 was made by using the catalyzed oxidation of N, N-diethyl-1,4-phenylenediammonium sulphate (DPD) by Horseradish peroxidase (POD)[40]. The absorption peaks at around 510 and 551 nm confirm the formation of H_2O_2 during the reaction process [Figure 3B]. The EPR and UV-Vis results indicate that the N-doped sp^3@sp^2 nanocarbon catalyzed aerobic synthesis of P was proceeding via superoxide radical ($O_2^{\bullet-}$) involved routine and H_2O_2 was formed as intermediate by hydrogen abstraction from the organic substrate directly or (in)directly. The activation process of I was also studied by ATR-IR [Figure 3C and Supplementary Figure 4] and the redshift (from 3329 cm^{-1} to 3324 cm^{-1}) of -OH group of I was observed in the presence of model catalyst[41]. The results indicate that I was activated by the catalysts and the -OH bond was weakened before the H abstraction step.

Based on the results above, a plausible reaction mechanism of intermolecular annulation reaction between 2-phenyl benzoxazole and benzyl aldehyde could be proposed. As shown in Figure 3D, initially, the intermediate I forms by the condensation of o-aminophenol and benzyl aldehyde. Then, the formed I absorbs on the catalyst's surface, and the reaction is initiated with a hydrogen abstraction step of the O-H bond from I by the catalyst. Then the I^* undergoes intramolecular cycloaddition of the imine to form the corresponding aminyl radical (P^*). The reaction is followed by the second H abstraction from the P^* due to the driving force for aromatization and ultimately generates the desired product [P]. Meanwhile, after the O_2 was absorbed on the surface of the catalyst, the electron transfer happened from the C atom adjacent to the pyridinic N to the O_2 to form O_2•$^-$, which subsequently react with the protons abstracted by the catalyst to form H_2O_2 and regenerate the active sites.

Substrate scope experiments

Having successfully achieved the aerobic oxidative synthesis of 2-phenyl benzoxazole, it is valuable to analyse how the catalytic system could be applied to synthesise other substituted benzoxazoles, benzothiazoles and benzothiazoles and benzimidazoles by using different substituted 2-aminophenol, 2-amino thiophenol or 2-phenylenediamine respectively with aldehydes as starting materials [Figure 4]. The reactions with benzaldehydes bearing electron-deficient [P2 and P3] and electron-rich groups [P4-P6] at the aromatic ring proceed smoothly to give the desired products in good yields. When the cinnamaldehyde [P7] and 4-formyl-trans-stilbene [P8] were chosen as reactants, the desired products were produced with yields of 92.6% and 84.4%, respectively. 82.9% yield of P9 was achieved when the furfural was chosen to provide

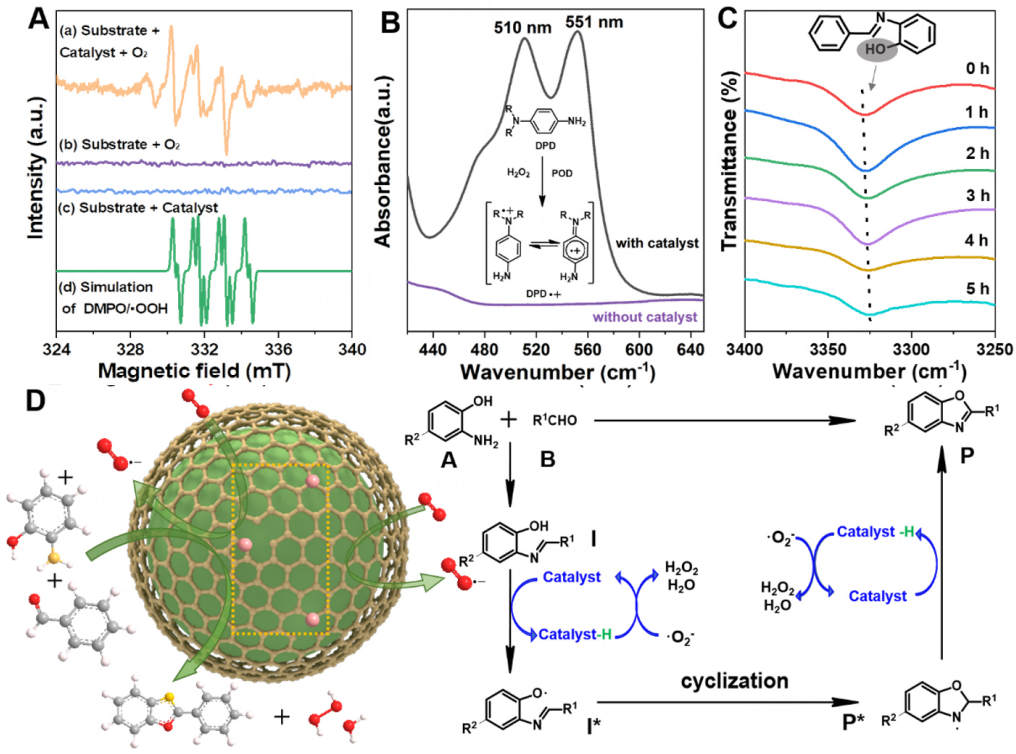

Figure 3. A: The EPR spectra of different reaction systems with DMPO as radical trap; B: The ultraviolet-visible absorption spectra of the reaction system (with and without catalyst) after adding DPD and POD; C: ATR-IR spectrum of catalytic systems with I as reactant, 1,10-phenanthroline as model catalyst and toluene as solvent under 140 °C in O_2 for 1, 2, 3, 4 and 5 h, respectively; D: Schematic representation of the proposed mechanism of N-doped sp^3@sp^2 nanocarbon catalyzed aerobic synthesis of 2-substituted benzoxazoles.

the aldehyde group. The aliphatic aldehydes were also successfully employed as substrates to give the corresponding products but with relatively lower yields [P10-P11]. After the aldehydes screening, the scope of various 2-aminophenols was also investigated. Functional groups including chloro, nitro, and cyano were well tolerated under the optimal reaction conditions, and the desired products were obtained in moderate to good yields [P12-P14]. The results above indicate that the reactions are insensitive to the electron-donating or election-withdrawing nature of the substitutes. A high yield of 73.3% was obtained when the benzene ring was replaced by a naphthyl group [P15].

To further validate the general use of the proposed catalytic method, the 2-aminophenols were replaced with 2-aminothiophenol and 2-phenylenediamine for synthesising benzothiazoles and benzimidazoles. To our delight, the reactions of 2-amino thiophenol and 2-phenylenediamine with benzaldehyde, furfural and benzaldehydes bearing chloro and methoxyl groups proceed with good yield as shown in Figure 4, P16-P22.

CONCLUSIONS

N-doped sp^3@sp^2 hybrid nanocarbons are fabricated as highly effective, stable and valuable metal-free carbocatalysts for the aerobic catalytic oxidative synthesis of various heterocycles, including 2-substituted benzoxazoles, benzothiazoles, and benzimidazoles with high yields, stability and broad substrate scope. The mechanistic study proves that the N-doped sp^3@sp^2 hybrid nanocarbons could activate O_2 molecules to yield superoxide radicals reacting with the abstracted proton on the catalyst's surface to form H_2O_2 while regenerating the catalyst. This study demonstrates that the N-doped sp^3@sp^2 hybrid catalytic system provides an attractive and useful methodology to achieve a green chemistry approach for the one-pot

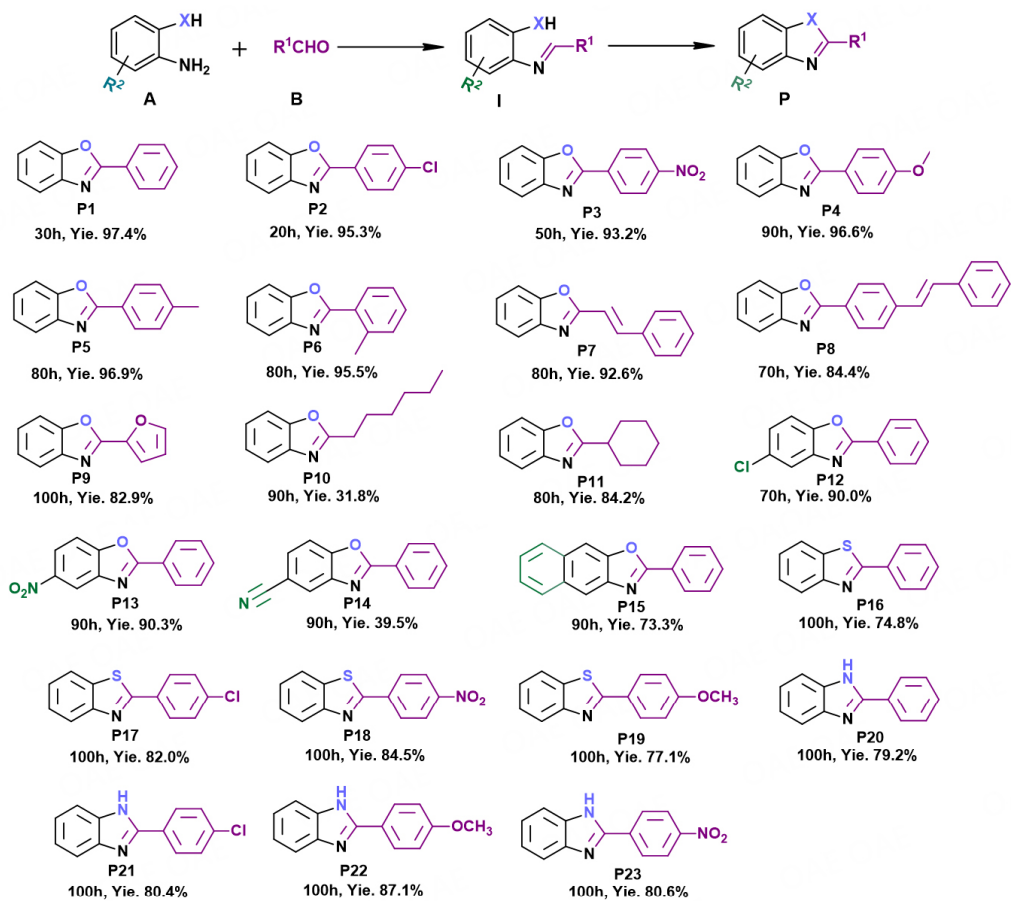

Figure 4. Substrate scope for aerobic synthesis of 2-substituted benzoxazoles, benzothiazoles and benzimidazoles. 2 mmol aminophenol, 2.2 mmol benzaldehyde, 10 mL xylene, 120 mg catalyst (NND900), 140 °C, 1 atm O_2; Isolated yield. The structures of all products were identified by the GC-MS [Supplementary Figure 5].

synthesis of important pharmaceutically related products.

DECLARATIONS

Acknowledgements

The authors acknowledge Mr. Hiroaki Matsumoto from Hitachi High-Tech for his great help in HR-TEM and EELS data acquisition at HF 5000 microscope. The authors thank Dr. Quan Li (Hubei University) for assistance with the NMR analysis. We sincerely cherish our memory of Prof. Dangsheng Su for his indispensable support and fruitful discussions.

Authors' contributions

Designed the study, conducted the experiments, data analysis and co-wrote the manuscript: Liu Y, Gu Q
Performed the catalysts synthesis, catalytic performance test and structural characterizations: Gu Q
Participated in the analysis of characterizations and revised the manuscript: Huang R, Xu C, Li S, Perathoner S, Centi G
Supervised the project: Liu Y, Centi G
Discussed the results and commented on the manuscript: Gu Q, Huang R, Xu C, Li S, Perathoner S, Centi G, Liu Y

Availability of data and materials
Not applicable.

Financial support and sponsorship
This work was financially supported by the National Key R&D Program of China (No. 2022YFC3701900); National Natural Science Foundation of China (Nos. 21872144, 21972140 and 22172161); LiaoNing Revitalization Talents Program (XLYC1907053) and Dalian National Laboratory for Clean Energy (DNL202021); S.P. and G.C. also thank the support from the CAS President's International Fellowship Initiative (PIFI) program.

Conflicts of interest
All authors declared that there are no conflicts of interest.

Ethical approval and consent to participate
Not applicable.

Consent for publication
Not applicable.

Supplementary Materials

REFERENCES
1. Liu X, Dai L. Carbon-based metal-free catalysts. *Nat Rev Mater* 2016:1. DOI
2. Su DS, Wen G, Wu S, Peng F, Schlögl R. Carbocatalysis in liquid-phase reactions. *Angew Chem Int Ed Engl* 2017;56:936-64. DOI
3. Li H, Li C, Wang Y, et al. Selenium confined in ZIF-8 derived porous carbon@MWCNTs 3D networks: tailoring reaction kinetics for high performance lithium-selenium batteries. *Chem Synth* 2022;2:8. DOI
4. Li S, Gu Q, Cao N, et al. Defect enriched N-doped carbon nanoflakes as robust carbocatalysts for H_2S selective oxidation. *J Mater Chem A* 2020;8:8892-902. DOI
5. Xu C, Gu Q, Li S, et al. Heteroatom-doped monolithic carbocatalysts with improved sulfur selectivity and impurity tolerance for H_2S selective oxidation. *ACS Catal* 2021;11:8591-604. DOI
6. Xu C, Chen J, Li S, et al. N-doped honeycomb-like porous carbon derived from biomass as an efficient carbocatalyst for H_2S selective oxidation. *J Hazard Mater* 2021;403:123806. DOI
7. Jia Y, Zhang L, Zhuang L, et al. Identification of active sites for acidic oxygen reduction on carbon catalysts with and without nitrogen doping. *Nat Catal* 2019;2:688-95. DOI
8. Yin Y, Kang X, Han B. Two-dimensional materials: synthesis and applications in the electro-reduction of carbon dioxide. *Chem Synth* 2022;2:19. DOI
9. Wu Q, Jia Y, Liu Q, et al. Ultra-dense carbon defects as highly active sites for oxygen reduction catalysis. *Chem* 2022;8:2715-33. DOI
10. Navalón S, Dhakshinamoorthy A, Álvaro M, García H. Diamond nanoparticles in heterogeneous catalysis. *Chem Mater* 2020;32:4116-43. DOI
11. Lin Y, Liu Z, Niu Y, et al. Highly efficient metal-free nitrogen-doped nanocarbons with unexpected active sites for aerobic catalytic reactions. *ACS Nano* 2019;13:13995-4004. DOI
12. Feng L, Ali S, Xu C, et al. Assessing the nature of active sites on nanodiamonds as metal-free catalysts for the EB-to-ST direct dehydrogenation using a catalytic approach. *ACS Catal* 2022;12:6119-31. DOI
13. Crane MJ, Petrone A, Beck RA, et al. High-pressure, high-temperature molecular doping of nanodiamond. *Sci Adv* 2019;5:eaau6073. DOI PubMed PMC
14. Huang F, Deng Y, Chen Y, et al. Atomically dispersed Pd on nanodiamond/graphene hybrid for selective hydrogenation of acetylene. *J Am Chem Soc* 2018;140:13142-6. DOI
15. Liu D, Li X, Chen S, et al. Atomically dispersed platinum supported on curved carbon supports for efficient electrocatalytic hydrogen evolution. *Nat Energy* 2019;4:512-8. DOI
16. Mochalin VN, Shenderova O, Ho D, Gogotsi Y. The properties and applications of nanodiamonds. *Nat Nanotechnol* 2011;7:11-23.

DOI

17. Liu Y, Chen S, Quan X, Yu H. Efficient electrochemical reduction of carbon dioxide to acetate on nitrogen-doped nanodiamond. *J Am Chem Soc* 2015;137:11631-6. DOI
18. Lin Y, Wu KT, Yu L, Heumann S, Su DS. Efficient and highly selective solvent-free oxidation of primary alcohols to aldehydes using bucky nanodiamond. *ChemSusChem* 2017;10:3497-505. DOI PubMed
19. Lin Y, Li B, Feng Z, Kim YA, Endo M, Su DS. Efficient metal-free catalytic reaction pathway for selective oxidation of substituted phenols. *ACS Catal* 2015;5:5921-6. DOI
20. Lin Y, Su D. Fabrication of nitrogen-modified annealed nanodiamond with improved catalytic activity. *ACS Nano* 2014;8:7823-33. DOI
21. Duan X, Su C, Zhou L, et al. Surface controlled generation of reactive radicals from persulfate by carbocatalysis on nanodiamonds. *Applied Catalysis B: Environmental* 2016;194:7-15. DOI
22. Lenarda A, Wirtanen T, Helaja J. Carbon Materials as catalytic tools for oxidative dehydrogenations and couplings in liquid phase. *Synthesis* 2023;55:45-61. DOI
23. Chen YX, Qian LF, Zhang W, Han B. Efficient aerobic oxidative synthesis of 2-substituted benzoxazoles, benzothiazoles, and benzimidazoles catalyzed by 4-methoxy-TEMPO. *Angew Chem Int Ed Engl* 2008;47:9330-3. DOI
24. Blacker AJ, Farah MM, Hall MI, Marsden SP, Saidi O, Williams JM. Synthesis of benzazoles by hydrogen-transfer catalysis. *Org Lett* 2009;11:2039-42. DOI PubMed
25. Yu J, Xu J, Lu M. Copper-catalyzed highly efficient aerobic oxidative synthesis of benzimidazoles, benzoxazoles and benzothiazoles from aromatic alcohols under solvent-free conditions in open air at room temperature: aerobic oxidative synthesis of benzimidazoles, benzoxazoles and benzothiazoles. *Appl Organometal Chem* 2013. DOI
26. Reddy MB, Nizam A, Pasha MA. $Zn(OAc)_2 \cdot 2H_2O$-catalyzed, simple, and clean procedure for the synthesis of 2-substituted benzoxazoles using a grindstone method. *Synthetic Commun* 2011;41:1838-42. DOI
27. Tang L, Guo X, Yang Y, Zha Z, Wang Z. Gold nanoparticles supported on titanium dioxide: an efficient catalyst for highly selective synthesis of benzoxazoles and benzimidazoles. *Chem Commun* 2014;50:6145-8. DOI
28. Yoo W, Yuan H, Miyamura H, Kobayashi S. Facile preparation of 2-substituted benzoxazoles and benzothiazoles via aerobic oxidation of phenolic and thiophenolic imines catalyzed by polymer-incarcerated platinum nanoclusters. *Adv Synth Catal* 2011;353:3085-9. DOI
29. Yu C, Guo X, Xi Z, et al. AgPd nanoparticles deposited on WO(2.72) nanorods as an efficient catalyst for one-pot conversion of nitrophenol/nitroacetophenone into benzoxazole/quinazoline. *J Am Chem Soc* 2017;139:5712-5. DOI
30. Duan X, Sun H, Wang S. Metal-free carbocatalysis in advanced oxidation reactions. *Acc Chem Res* 2018;51:678-87. DOI PubMed
31. Navalon, A. Dhakshinamoorthy, M. Alvaro, H. Garcia. Carbocatalysis by graphene-based materials. *Chem Rev* 2014;114:6179-6212. DOI
32. Hu F, Patel M, Luo F, et al. Graphene-catalyzed direct friedel-crafts alkylation reactions: mechanism, selectivity, and synthetic utility. *J Am Chem Soc* 2015;137:14473-80. DOI
33. Yang H, Cui X, Dai X, Deng Y, Shi F. Carbon-catalysed reductive hydrogen atom transfer reactions. *Nat Commun* 2015;6:6478. DOI
34. Zhang J, Liu X, Blume R, Zhang A, Schlögl R, Su DS. Surface-modified carbon nanotubes catalyze oxidative dehydrogenation of n-butane. *Science* 2008;322:73-7. DOI
35. Kawashita Y, Nakamichi N, Kawabata H, Hayashi M. Direct and practical synthesis of 2-arylbenzoxazoles promoted by activated carbon. *Org Lett* 2003;5:3713-5. DOI PubMed
36. Frank B, Morassutto M, Schomäcker R, Schlögl R, Su D. Oxidative dehydrogenation of ethane over multiwalled carbon nanotubes. *ChemCatChem* 2010;2:644-8. DOI
37. Guo D, Shibuya R, Akiba C, Saji S, Kondo T, Nakamura J. Active sites of nitrogen-doped carbon materials for oxygen reduction reaction clarified using model catalysts. *Science* 2016;351:361-5. DOI PubMed
38. Zhang C, Li T, Zhang J, Yan S, Qin C. Degradation of p-nitrophenol using a ferrous-tripolyphosphate complex in the presence of oxygen: the key role of superoxide radicals. *Appl Catal B* 2019;259:118030. DOI
39. Yamakoshi Y, Sueyoshi S, Fukuhara K, Miyata N, Masumizu T, Kohno M. •OH and $O_2^{\bullet-}$ generation in aqueous C_{60} and C_{70} solutions by photoirradiation: an EPR study. *J Am Chem Soc* 1998;120:12363-4. DOI
40. Su C, Acik M, Takai K, et al. Probing the catalytic activity of porous graphene oxide and the origin of this behaviour. *Nat Commun* 2012;3:1298. DOI
41. Doroshenko I, Pogorelov V, Sablinskas V. Infrared absorption spectra of monohydric alcohols. *Dataset Papers in Chemistry* 2013;2013:1-6. DOI